NASA/TM-20205010120

Toward Realizing the Potential of Practical Li-O_2 Batteries for Electric Aircraft

William R. Bennett and Donald Dornbusch
Glenn Research Center, Cleveland, Ohio

Kristian B. Knudsen
University of California, Berkeley, California

Mohit R. Mehta
KBR Wyle Services, LLC, Moffett Field, California

Bryan D. McCloskey
University of California, Berkeley, California

John W. Lawson
Ames Research Center, Moffett Field, California

December 2020

NASA STI Program . . . in Profile

Since its founding, NASA has been dedicated to the advancement of aeronautics and space science. The NASA Scientific and Technical Information (STI) Program plays a key part in helping NASA maintain this important role.

The NASA STI Program operates under the auspices of the Agency Chief Information Officer. It collects, organizes, provides for archiving, and disseminates NASA's STI. The NASA STI Program provides access to the NASA Technical Report Server—Registered (NTRS Reg) and NASA Technical Report Server—Public (NTRS) thus providing one of the largest collections of aeronautical and space science STI in the world. Results are published in both non-NASA channels and by NASA in the NASA STI Report Series, which includes the following report types:

- TECHNICAL PUBLICATION. Reports of completed research or a major significant phase of research that present the results of NASA programs and include extensive data or theoretical analysis. Includes compilations of significant scientific and technical data and information deemed to be of continuing reference value. NASA counter-part of peer-reviewed formal professional papers, but has less stringent limitations on manuscript length and extent of graphic presentations.

- TECHNICAL MEMORANDUM. Scientific and technical findings that are preliminary or of specialized interest, e.g., "quick-release" reports, working papers, and bibliographies that contain minimal annotation. Does not contain extensive analysis.

- CONTRACTOR REPORT. Scientific and technical findings by NASA-sponsored contractors and grantees.

- CONFERENCE PUBLICATION. Collected papers from scientific and technical conferences, symposia, seminars, or other meetings sponsored or co-sponsored by NASA.

- SPECIAL PUBLICATION. Scientific, technical, or historical information from NASA programs, projects, and missions, often concerned with subjects having substantial public interest.

- TECHNICAL TRANSLATION. English-language translations of foreign scientific and technical material pertinent to NASA's mission.

For more information about the NASA STI program, see the following:

- Access the NASA STI program home page at http://www.sti.nasa.gov

- E-mail your question to help@sti.nasa.gov

- Fax your question to the NASA STI Information Desk at 757-864-6500

- Telephone the NASA STI Information Desk at 757-864-9658

- Write to:
  NASA STI Program
  Mail Stop 148
  NASA Langley Research Center
  Hampton, VA 23681-2199

NASA/TM-20205010120

Toward Realizing the Potential of Practical Li-O_2 Batteries for Electric Aircraft

William R. Bennett and Donald Dornbusch
Glenn Research Center, Cleveland, Ohio

Kristian B. Knudsen
University of California, Berkeley, California

Mohit R. Mehta
KBR Wyle Services, LLC, Moffett Field, California

Bryan D. McCloskey
University of California, Berkeley, California

John W. Lawson
Ames Research Center, Moffett Field, California

National Aeronautics and
Space Administration

Glenn Research Center
Cleveland, Ohio 44135

December 2020

Acknowledgments

The authors gratefully acknowledge NASA's Convergent Aeronautics Solutions Project for its sponsorship of the Lithium Oxygen Batteries for NASA Electric Aircraft (LION) project.

This work was sponsored by the
Transformative Aeronautics Concepts Program.

Level of Review: This material has been technically reviewed by technical management.

Available from

NASA STI Program
Mail Stop 148
NASA Langley Research Center
Hampton, VA 23681-2199

National Technical Information Service
5285 Port Royal Road
Springfield, VA 22161
703-605-6000

This report is available in electronic form at http://www.sti.nasa.gov/ and http://ntrs.nasa.gov/

Toward Realizing the Potential of Practical Li-O_2 Batteries for Electric Aircraft

William R. Bennett and Donald Dornbusch
National Aeronautics and Space Administration
Glenn Research Center
Cleveland, Ohio 44135

Kristian B. Knudsen
University of California
Berkeley, California 94720

Mohit R. Mehta
KBR Wyle Services, LLC
Moffett Field, California 94035

Bryan D. McCloskey
University of California
Berkeley, California 94720

John W. Lawson
National Aeronautics and Space Administration
Ames Research Center
Moffett Field, California 94035

Abstract

Electrochemical power sources based on the Li-O_2 couple have potential to achieve more than two times the specific energy that is achievable with state-of-the-art Li-ion technologies. Despite considerable research, significant practical limitations continue to impede the successful realization of the Li-O_2 electrochemistry as a power source in electric and hybrid-electric aviation. In practice, power capability and cycle life present formidable challenges. In this work, projections are presented for Li-O_2 prismatic cells with lightweight construction and the effect of cathode-limited capacity and discharge rate on specific energy and power are presented. A laboratory-scale (4-W/12-V) Li-air battery pack was assembled and discharged under a notional electric flight power cycle. Factors that impact safety and limit pack performance are discussed, and concepts for future developments, which could enhance the rate capability are presented.

Nomenclature

ASI	area-specific impedance
DME	dimethoxyethane
FS	freestanding
GDL	gas diffusion layer
JANAF	Joint Army, Navy, and Air Force
LiTFSI	lithium bis(trifluoromethanesulfonyl)imide
MPL	microporous layer
RTIL	room-temperature ionic liquid
TEGDME	Tetraethylene glycol dimethyl ether
UAV	unmanned aerial vehicle

1.0 Introduction

Realizing the promise of green aviation with energy-efficient, low-noise, low-emission electric vehicles will require substantial technology leaps over current state-of-the-art battery chemistries. Electric aircraft represent perhaps the most demanding set of requirements of any battery application. Threshold values for general aviation are quoted as 400 Wh kg^{-1} whereas 750+ Wh kg^{-1} is expected for more ambitious vehicles, for example, regional service (Ref. 1). In addition to specific energy, other requirements are critical as well including specific power, rechargeability, safety, recharge time, cost, and others.

Benefiting from over 25 years of development, Li-ion technology presently achieves cell-level specific energy greater than 250 Wh kg^{-1} (Ref. 2). Yet, Li-ion is approaching a limit in performance, where only incremental improvements are possible, and there is a need for energy storage technology beyond Li-ion, especially to enable demanding applications such as electric air vehicles. To this end, battery technologies based on lithium metal have received considerable attention (Refs. 3 and 4). Non-aqueous Li-O_2 chemistry in particular—with a theoretical specific energy of 3,457 Wh kg^{-1}—appears to have significant promise at first inspection. However, this theoretical value assumes only the mass of the chemical reactants necessary to form the lithium peroxide reaction product, Li_2O_2, neglecting the essential auxiliary materials that are required to form a practical cell. Still other parasitic masses and auxiliary power requirements are imposed at the system level, with the result that the system possesses significantly less than the theoretical specific energy, when assembled in a cell structure that can generate sufficient electrical power to support electric aviation. It was the goal of this project to understand the limiting factors that govern specific energy in practical Li-O_2 cells and demonstrate 400 Wh kg^{-1} at the pack level.

While the metric of specific energy appears to be attractive for Li-O_2, specific power (W kg^{-1}) is a critical parameter for most practical applications but has received less attention in the literature. Energy density (Wh L^{-1}) at the system level is significant in electric propulsion applications where payload volume must be preserved. The significance of these metrics in practical automotive and electric aviation systems is discussed in the literature (Refs. 5 to 8).

With these challenges in mind, NASA recently sponsored the Lithium Oxygen Batteries for NASA Electric Aircraft (LION) project to evaluate the most significant issues in developing Li-O_2 systems into a practical battery technology for electric aircraft. Many issues are related to the well-known electrolyte and cathode decomposition, which places severe limitations on reversibility and capacity. Alternative materials were considered for carbon cathodes and ether-based electrolytes that are common in the literature. For example, high-stability molten salt electrolytes and oxide cathode coatings showed promise to control the severe decomposition (Refs. 9 and 10). However, even if stability issues are resolved, significant challenges remain to achieve the very high practical specific energy and specific power needed for electric aircraft. For example, the theoretical energy for Li-O_2 is widely cited; however, as far as we know, a reliable and complete accounting of the specific energy achievable in practical, laboratory-based cells has so far not been attempted. Further, an investigation of pack-level issues, specifically as related to integration and performance within an aircraft system has also not been attempted.

In this report, we will address both issues. First, based on laboratory Li-O_2 cell data, we estimate specific energy and power for these systems. We find that the role of the cathode is crucial, and the twin goals of optimizing effective cathode surface area and reducing cathode mass are key to achieving high performance. For this purpose, we utilize a homemade research carbon cathode that while certainly not optimized for high energy and power densities, nonetheless, is representative of the state-of-the art carbon-based oxygen cathodes examined in the open literature. Data from these cells was used to generate practical (and optimistic) estimations of specific energy and power. The calculations presented in this

summary represent the discharge characteristics of fresh cells at beginning of life. Considerations of charging processes and related decomposition processes are reviewed elsewhere (Ref. 11). Second, we built and evaluated a Li-O_2 battery pack appropriate for demonstration purposes for an electric aircraft test vehicle. Again, we find that the cathode is crucial. In this case, large cathode active area is required to achieve enough current to satisfy power requirements. It was clear that homemade research cathodes could not be scaled up to satisfy the demands of the demonstration cell activity. Therefore, commercial carbon fuel cell materials, which are readily available in sufficient sheet sizes, were selected for demonstration activities. These substitute materials satisfied the desired power levels for demonstration but developed low cell-level specific energy and power due to the unoptimized character of the materials. Cell and pack designs were considered, built, and evaluated according to an electric aircraft flight profile. We show that the Li-O_2 pack considered was able to execute a scaled-down flight profile, albeit at very low power density (W kg^{-1}). Cathode optimization will again be crucial to achieving higher power levels in future studies. Finally, based on these analyses supplemented with results from a recent battery multiphysics study, we make projections about what may be achieved from properly optimized Li-O_2 cells and packs with enough optimization and improvements in materials and component design.

2.0 Theory and Calculation

2.1 Li-O_2 Theoretical Limits

The overall Li-O_2 cell reaction in organic electrolyte demonstrates a 2-electron transfer per mole of O_2, to produce the insoluble lithium peroxide product Li_2O_2 (Ref. 12):

$$2Li + O_2 \leftrightharpoons Li_2O_2 \tag{1}$$

Relevant theoretical properties for reaction (1) appear in Table 1. Based on the Gibbs free energy change, ΔG, the theoretical specific energy is 571 kJ $mole^{-1}$ Li_2O_2, or 3,457 Wh kg^{-1} Li_2O_2. The reversible cell voltage, E^o, is 2.96 V ($\Delta G = -nFE^o$). The thermoneutral voltage, V_{th}, is computed from the enthalpy change, ΔH, in a fashion analogous to the reversible voltage: V_{th} = 3.28 V ($\Delta H = -nFV_{th}$). This parameter has significance for computing thermal efficiency and heat generation but is rarely mentioned in the Li-O_2 literature. The ratio of free energy and enthalpy of formation dictates the maximum theoretical efficiency: for reaction (1) $\Delta G/\Delta H$ = 90 percent. The V_{th} is valuable for calculating efficiency and waste heat production from the cell operating voltage. For example, a cell with a discharge voltage of 2.5 V has an energy efficiency of 2.5/3.28 = 76 percent. A simplified calculation for heat generation at a given discharge current, I, is performed readily using the difference between V_{th} and the observed cell voltage, E_{obs}:

$$Q_{gen} = I\left(V_{th} - E_{obs}\right) \tag{2}$$

Equation (2) assumes discharge current as positive, and heat flow from the cell to the environment, Q_{gen}, as positive. Thus, a cell supporting a 1 A discharge current at 2.5 V produces 2.5 W_{el} of electrical power, while generating Q_{gen} = 0.78 W_{th} of waste heat.[1] Equation (2) is applicable to a cell under charge, provided the current is taken as negative. It is noteworthy that reaction (1) will be endothermic on charge at cell voltages less than the thermoneutral voltage, E_{obs} < 3.28 V, requiring heat to be added from the

[1] Q_{gen} = 1 A × (3.28 – 2.5) V = 0.78 W_{th}. This is consistent with a 76 percent energy efficiency: 2.5/(2.5 + 0.78) = 0.762.

TABLE 1.—FUNDAMENTAL AND THEORETICAL PROPERTIES. THERMODYNAMIC PROPERTIES FROM JANAF THERMOCHEMICAL TABLES, 2nd EDITION, 1970. THERMODYNAMIC PROPERTIES ARE REFERENCED TO 25 °C AND 1 atm.

	Mw, g mol^{-1}	S^o, J/ mol^{-1} K^{-1}	$\Delta H_f{}^o$, kJ mol^{-1}	$\Delta G_f{}^o$, kJ mol^{-1}	Specific capacity, mAh g^{-1}	E^o, V	Specific energy, Wh kg^{-1}
Li_2O_2	**45.88**	**56.484**	**–632.621**	**–570.982**	**1,168**	**2.959**	**3,457**
O_2	31.9988	205.033	0	0	1,675	-------	-------
Li (s)	6.94	29.096	0	0	3,862	-------	-------

Theoretical specific energy based on Li: 3,862 × 2.96 = 11,432 Wh kg^{-1} Li.

Theoretical specific energy based on Li plus O_2: 1,168 × 2.96 = 3,457 Wh kg^{-1}.

environment in order for the charge reaction to proceed. This is consistent with the relatively high charge voltage that is observed in laboratory cells, which operate at ~3.3 V at the onset of charge. More importantly, this dictates that attempts to reduce the cell charging voltage below 3.28 V would provide no net benefit to the energy efficiency of the cell, since any such savings in electrical energy input would be offset by a thermal energy requirement.

2.2 Electrode Structure and Discharge Limitations

The physical structure of the oxygen cathode is illustrated in Figure 1. The hypothetical cathode structure (a) consists of a porous carbon layer, which is partially wetted with electrolyte. Here, a network of open porosity is available for gas-phase oxygen diffusion to active sites throughout the cathode structure, where it dissolves locally into the electrolyte to support the oxygen reduction reaction. This ideal condition is approached in metal-air cells with aqueous electrolyte, where hydrophobic additives in the carbon (e.g., poly(tetrafluoroethylene) (PTFE)) help to preserve three-phase boundaries for cell reaction (Refs. 13 to 15). In contrast, organic electrolytes readily wet and fill the cathode structure, making it difficult to preserve open channels for gas-phase diffusion. This produces the flooded electrode geometry illustrated in Figure 1(b). Here, oxygen transport is restricted to slower, liquid-phase diffusion of dissolved species. This limits the rate of discharge (current density, A m^{-2}) and power density (W m^{-2}). Gains in current density and power density may be achieved if more three-phase interfacial contact could be promoted in the cathode structure (Ref. 16).

As discharge progresses, solid Li_2O_2 product accumulates within the cathode pore structure, as suggested in Figure 1. The morphology of the deposit is influenced by electrolyte type and current density, ranging from thin films to corpuscular toroidal structures (Refs. 17 to 19). Continued deposition of Li_2O_2 blocks the pore structure and obscures cathode active sites, ultimately limiting discharge capacity. Because of this limiting character, an apparent “capacity” can be assigned to the cathode material, even though it does not directly participate in the discharge reaction.

2.3 Air Versus Oxygen

An examination of the relative merits of Li-O_2 and Li-air batteries, reveals some tradeoffs. Design for operation with air, while attractive where air is available, introduces contamination issues along with a minor reduction in cell voltage and rate capability. Carbon dioxide competes with oxygen, forming an extremely stable Li_2CO_3 discharge product, which is not readily decomposed on charge (Ref. 20). Irreversible carbonate accumulation will eventually limit cell life. Moisture can be expected to dissolve readily in hygroscopic organic electrolytes where it would eventually react irreversibly with the

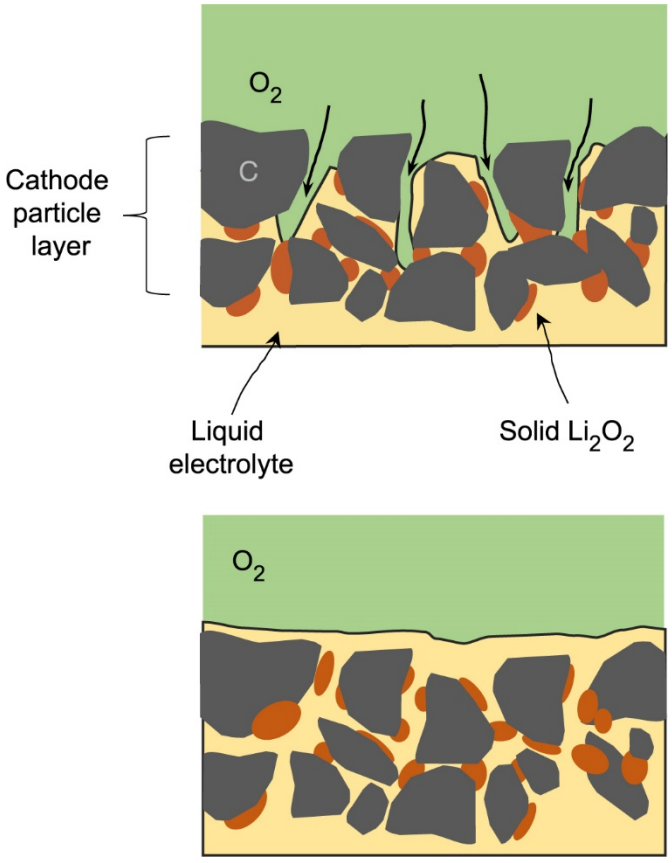

Figure 1.—(a) Cathode with open pores to facilitate O_2 gas transport to active sites. (b) Cathode with pores flooded by liquid electrolyte.

Li electrode, consuming cell capacity. Similarly, moisture will react chemically with the Li_2O_2 discharge product leading to additional capacity loss. These parasitic processes suggest the need for purification of ambient air for intake in Li-air applications, which ultimately require a more complicated system.

In addition to competitive reaction of CO_2 and H_2O at the cathode surface, significant decomposition also plays a role in traditional carbon cathode-organic solvent Li-O_2 systems. The reactants and intermediates occurring through the reduction of oxygen are highly reactive, attacking and degrading organic molecules (Ref. 21) and carbon cathodes (Refs. 22 and 23). The decomposition products can be soluble and insoluble, inhibiting transport to the cathode surface or accumulating on the cathode surface and decreasing active area (Refs. 24 to 26). Lithium carbonate is the primary decomposition product from both electrolyte and carbon degradation, which forms a passivating layer that is resistant to oxidation and is highly insulating against electron transport, limiting deposition sites for Li_2O_2 and preventing electron access to dissolved O_2 in the electrolyte. This passivation effect contributes significantly to the poor cycle life and high overpotential on charge. High charging voltages also lead to further electrolyte decomposition when forced above the organic electrolyte stability window. Despite significant research to improve the stability of organic electrolytes (Refs. 9, 27 to 33), further progress is needed in order to achieve high enough efficiency to operate thousands of cycles. However, the carbon cathode-organic electrolyte remains the best studied system for this chemistry and are used for cell development in this report.

Furthermore, evaporation of electrolyte solvent is another practical issue in both Li-O_2 and Li-air systems but may be especially problematic in Li-air batteries with volatile organic-based electrolytes where excess air must be circulated through the cell, drawing significant solvent away over time. Some

discussion of air purification and other issues related to automotive applications are presented by Greszler (Ref. 34). In contrast, closed oxygen-based systems help address the contamination and evaporation issues but require pressurized oxygen storage and safety elements, which add to the complexity and mass at the system level. Moreover, the reactivity of oxygen with cell materials in the presence of flammable electrolyte solvents poses a significant concern, particularly if the oxygen is introduced to the cell at elevated pressure. A simple closed design that is analogous to the nickel-hydrogen battery with individual pressure vessels could be constructed, which offers a potentially attractive approach (Ref. 35). Such closed designs would house the electrodes in a sealed pressure vessel, with internal oxygen pressure varying with state of charge. This approach could lead to relatively simple battery designs with open cells that "breathe" pressurized oxygen enclosed inside a common pressurized vessel. While attractive in terms of simplicity, a battery design that houses flammable lithium metal, electrolyte, and carbon inside a vessel pressurized with oxygen would pose considerable risk. Relevant safety issues for Li-O_2 battery design can be found in the NASA safety standard for oxygen systems (Ref. 36).

Gallagher et al. present perspectives of the closed and open system design characteristics as they relate to electric automotive applications (Ref. 6). Protection of the lithium metal from oxygen gas or dissolved oxygen would be problematic in both air-fed and oxygen-fed systems. A cell geometry for protecting lithium from such contamination is considered in a design described by Park et al. (Ref. 37). An in-depth analysis of the O_2 versus air tradeoff is beyond the scope of this report but will surely be an important factor in system design.

2.4. Electrolyte Selection and Safety Concerns

The choice of electrolyte requires careful consideration of electrochemical stability, chemical stability under exposure to oxygen, transport properties, safety, and volatility. Electrolyte screening formed a substantial portion of this NASA Convergent Aeronautics Solutions (CAS)-funded activity and details of that work are described elsewhere (Refs. 38 to 40). Here, we discuss practical consideration related to solvent evaporation and safety. Since the Li-O_2 cathode necessarily requires a gas interface, there is an avenue for solvent evaporation into the supporting gas stream, which is particularly problematic in open systems that require passive diffusion or forced flow of air. Closed oxygen-based systems would limit evaporative loss by eliminating the need for flow-through of air, but some exchange of solvent vapor would remain, particularly during charge when generated oxygen gas flows out of the cells. Tetraethylene glycol dimethyl ether (TEGDME) was used as an electrolyte solvent for cell scale-up demonstrations in this work, due to low vapor pressure (<0.01 mmHg at 20 °C), high flash point (141 °C), and high ignition temperature (266 °C). Safety data sheets for the ether-based solvents (dimethoxyethane (DME) is frequently used) suggest that these solvents can form explosive organic peroxides on prolonged storage in air. This potential hazard needs to be addressed before making an electrolyte solvent selection. In this regard, nonorganic electrolytes such as room-temperature ionic liquids (RTILs) or molten salt electrolytes could offer benefits in reducing evaporative losses and may eliminate the risk of organic peroxide formation.

An additional safety concern is the potential for developing flammable atmospheres consisting of electrolyte solvent vapor and oxygen (or air) in the Li-O_2 cell. Such cells present two elements of the "fire triangle," and an ignition source, such as a spark from a poor electrical connection, could lead to explosion or fire. This consideration must be considered in selecting an electrolyte solvent for use in a practical system. Flammability hazards represent another issue, which may make nonflammable inorganic electrolytes desirable in Li-O_2 applications.

3.0 Experimental Methods

3.1 Experimental Cathode Preparation and Performance

It was noted previously that the cathode structure influences the capacity, which can be achieved at useful rates. Much of the reported cathode work has been performed with carbon black, largely without additional catalyst. Indeed, the role of catalyst is controversial, with evidence suggesting that catalysts can accelerate the degradation of both cathode and electrolyte (Ref. 41). Discharge data collected in our laboratory for experimental cathodes using two different Vulcan® XC72 (Cabot Corporation) carbon-black-based electrodes appear in Figure 2. The sprayed XC72 cathodes were prepared similarly to the procedures described in references (Refs. 3 and 42) while the freestanding (FS) cathodes were prepared as follows. A mixture of Vulcan® XC72 (purchased from Fuel Cell Earth) was mixed with 5 wt% PTFE

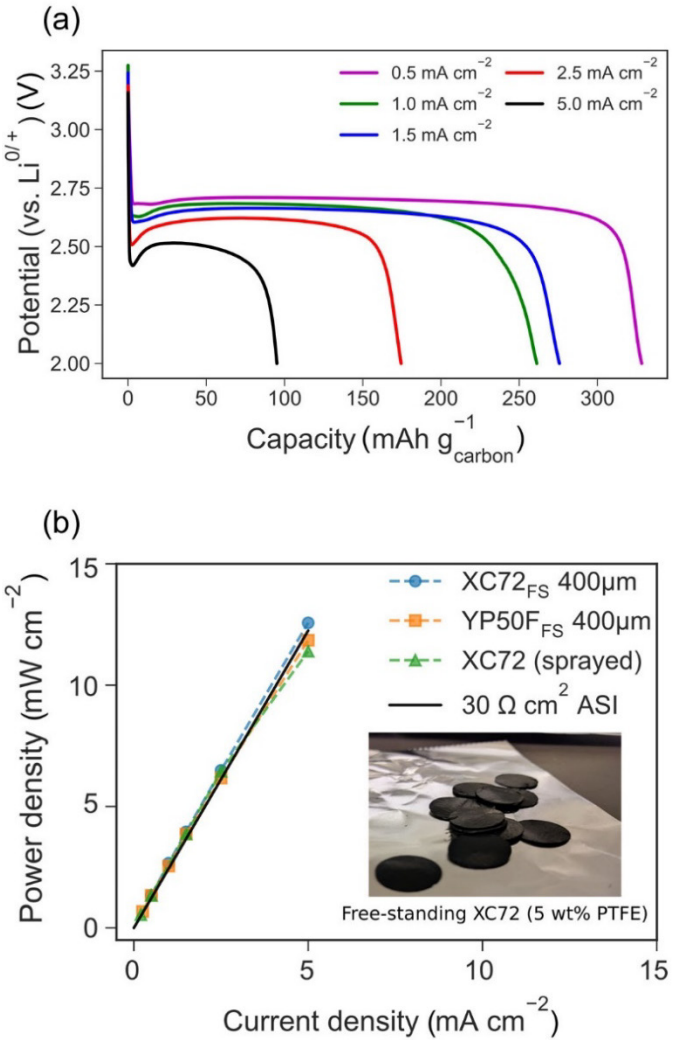

Figure 2.—(a) Discharge capacity of freestanding XC72 experimental carbon black oxygen electrodes, (b) areal power density based on plateau voltage for three different carbon black materials. Solid black line represents power projection for 2.6 V open circuit potential in series with 30 Ω-cm² area-specific impedance. Cabot Corporation $XC72_{FS}$ research cathodes (freestanding 400-μm by 12-mm diameter discs) shown in inset.

binder (Sigma-Aldrich) in 4:1 isopropyl alcohol and deionized water and stirred vigorously until the solvent evaporated. The doughy material was kneaded and pressed into a thickness of 400-μm and were punched into 12-mm-diameter disks, then dried in vacuum at 110 °C for 12 h, transferred to a glovebox, and placed on a hotplate at 200 °C prior to use.

The Li-O_2 cells were assembled using an in-house leak tight system based on Swagelok® components, with precise volumes as described elsewhere (Ref. 42), inside an Ar-filled glovebox with <0.1 ppm H_2O and O_2. The cells were fabricated with the 12-mm XC72 carbon-based cathodes, a 1/2-in. Whatman QMA glass fiber separator with 80 μL of electrolyte (1 M lithium bis(trifluoromethanesulfonyl)imide (LiTFSI) in DME (BASF)), and a 12-mm lithium disk (MTI Corporation) as the anode. Each cell was leak tested prior to investigations and cells were maintained at a pressure ~1,200 torr of O_2 during discharge.

4.0 Projections for a Hypothetical Li-O_2 Cell

Here, we project the specific energy and power for a practical Li-O_2 cell design. Mass estimates make allowance for separator, electrolyte, excess lithium electrode capacity, current collectors and tabs, oxygen flow field, and cell case materials. Specific energy and specific power are calculated with current density as a parameter, using optimistic assumptions for the rate capability and cell voltage. These estimates illustrate the significance of cathode rate capability and suggest practical limits for the Li-O_2 chemistry. The prospective cell design described here represents one approach for constructing cells with power capability suitable for electric aviation. Other construction methods and physical assumptions may be possible.

4.1 Electrode Assumptions

Consider a Li-O_2 battery that is required to deliver 400 W for 1 h, at a nominal voltage of 24 V. The corresponding discharge current (assumed constant) is equal to 16.7 A. For a cell discharge potential of approximately 2.5 V, the hypothetical 24-V battery would require 10 cells in series. We assume that the discharge properties of the cathode are the limiting factors for this design, and that the Li anode can support a current density that is significantly greater than the limiting current density of the cathode. The what-if analysis that follows projects specific energy and power density for the 16.7 Ah cells, use hypothetical values for the specific capacity of the cathode material (mAh g^{-1}) and electrode capacity loading (mAh cm^{-2}). These parameters establish the electrode dimensions (projected electrode area), cell mass, and volume. Cathode layer thickness was computed to satisfy the desired capacity loading with allowance for porosity. Loadings of 2, 4, and 8 mAh cm^{-2} are explored in these hypothetical calculations. Early commercial Li-ion cells have typically been designed with capacity loading of approximately 2.4 to 3.4 mAh cm^{-2} (Ref. 43). In-house measurements of high-energy LG Chem INR18650 MJ1 3500 mAh cells reveal an electrode area of approximately 720 cm^2 with an associated capacity loading of 4.9 mAh cm^{-2}. Based on this electrode area, the LG Chem INR18650 MJ1 cell reaches 13.9 mA cm^{-2} at its 10 A maximum rated discharge current.

Power and energy are calculated using a range of discharge current densities (mA cm^{-2}), assuming a simple linear relationship for discharge voltage. For what-if analysis, we adopt a linear relationship for the cell voltage based on the discharge plateau potentials in Figure 2, assuming an open circuit potential of 2.6 V with area-specific impedance of 30 Ω-cm^2. This empirical projection for cell voltage omits kinetic and transport limitations, allowing for future improvement to the rate performance of the oxygen cathode. The apparent area-specific impedance (ASI) of 30 Ω-cm^2 is consistent with observed initial impedance reported in Reference 37 for a high-specific energy cell design. These projections are presented merely to illustrate the bounds for cell-level specific energy and power, which could be achieved given hypothetical cathode performance. In some of these cases, the capacity loading could lead

to excessive electrode thickness with transport limitations that are inconsistent with the assumed current density. Projections are extrapolated up to 40 mA cm^{-2}, which corresponds to the approximate maximum power that can be achieved with the assumed linear polarization behavior with 30 Ω-cm^2 (Figure A.3). See Appendixes for additional details.

Cathode material calculations assume carbon black (2.2 g cm^{-3}) as active material, with PVdF binder. We assume that the cathode thickness provides adequate pore volume to completely contain the theoretical solid volume of Li_2O_2 produced in discharge. At 16.7 Ah, the hypothetical cell will consume 10 g of oxygen, and produce 14.3 g of Li_2O_2, requiring 6.18 cm^3 of cathode pore volume. The estimates presented here allow for 110 percent of the theoretical volume in porosity. Cathode porosity is dependent on the specific capacity of the carbon active material, ranging from approximately 40 to 80 percent, for 1,000 and 5,000 mAh g^{-1}, respectively. Capacities as high as 5,000 mAh g^{-1} have been reported in the literature (Ref. 44). With total cell capacity established, cathode mass is determined by the specific capacity of the active material.

Cell mass calculations allow for 25 percent excess electrolyte, in addition to that required to fill the pore volume of the cathode and separator layers. We assume electrolyte density of 1M LiTFSI in TEGDME for these estimates. Thin polyethylene separator material (16 μm) with 35 percent porosity is assumed for making these mass and volume estimates. Electrodes use 25-μm-thick expanded metal (e.g., Dexmet Corporation Microgrid®) current collecting foil: aluminum and copper material for the cathode and anode, respectively. Commercially available materials, with ~40 percent open area, provide a significant mass savings relative to solid foil sheet and are particularly suitable for the cathode current collector, which requires open area for gas transport. Microgrid® foils were used in the demonstration cells assembled for this work.

Negative electrode material is assumed to be constructed of solid lithium metal foil, with theoretical specific capacity (3.862 Ah g^{-1} Li) and density (0.53 g cm^{-3}). The designs allow for excess Li, using a positive-to-negative capacity ratio, P/N = 0.8; therefore, the lithium foil thickness is 1.25 times thicker than the stoichiometric amount. This allowance helps to assure that a residual layer of unreacted lithium remains after discharge, providing a host surface for lithium plating on charge, and to accommodate minor nonuniformities in current density distribution. In addition, cell mass calculations allow for the negative electrode to be oversized relative to the positive electrode by 1.5 mm on each edge. This measure increases the tolerance for minor misalignment of electrodes inside the finished cell and assures that the positive electrode is everywhere opposed by negative electrode material.

4.2 Prismatic Cell Construction

Assuming operation at 1 mA cm^{-2}, the hypothetical cell requires nearly 1.7 m^2 of electrode area to support a discharge current of 16.7 A. A prismatic cell design, using multiple electrode leaves, provides a practical means of building large electrode area in a compact volume. This approach uses a double-sided lithium anode, sealed in a pouch of separator material, with an oxygen electrode disposed on each face to form a bicell element. A flow field is required to distribute oxygen (or air) to the gas side of the cathode. Cathodes, arranged back-to-back, would logically share a flow field in building the multileaf stack. This structure is illustrated in Figure 3. Positive and negative electrode tabs are joined building parallel connections between the bicell elements. In this way, 1.7 m^2 of electrode area can be built up using

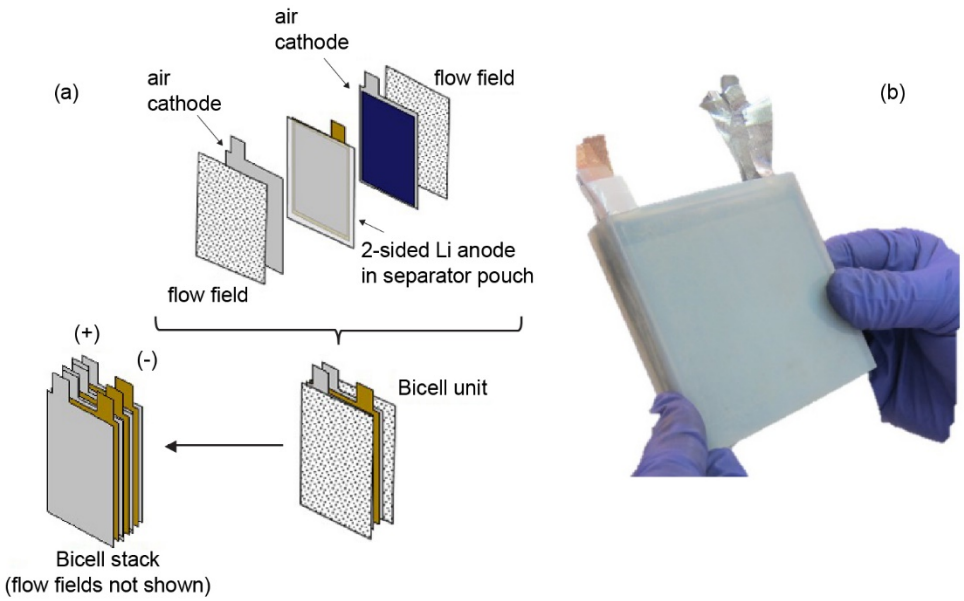

Figure 3.—(a) Prismatic cell construction using bicell elements to build active area. (b) 470 cm² demonstration cell with three bicell elements in plastic cell case. Tab connections, flow-field material, and case add to the parasitic cell mass.

30 bicell elements with dimensions of 20 by 14 cm. Cell size calculations assume the bicell elements have a 1.5:1 aspect ratio, with the gas diffusion path along the 14-cm dimension.

Design considerations for the gas flow field will vary depending on the required current density, path length, and choice of oxygen or air as the depolarizing gas. Here, we assume a passive airbreathing cell designed for natural convection and diffusion of ambient air to the cathode. A 1.6-mm- (1/16-in.-) thick layer of reticulated polyester foam sheet is assumed for preliminary estimates. This choice of material also provides resilient compression for maintaining electrode interfacial contact during charge and discharge.

Estimates for cell mass include tab and terminal materials for electrically joining the bicells, and a lightweight enclosure material similar to that used for constructing pouch cells. Lastly, we include the stoichiometric weight of oxygen (0.60 g O_2 Ah^{-1}) in completing estimates for the finished cell mass. Oxygen consumption represents a significant contribution to the discharged cell mass, approximately 2.3 times the stoichiometric mass of Li. The 16.7 Ah cell consumes approximately 10 g of oxygen to form the Li_2O_2 discharge product.

4.3 Cell-Level Performance Projections

The following projections assume carbon specific capacity of 1,000, 3,000, and 5,000 mAh g^{-1} C with loadings of 2, 4, and 8 mAh cm^{-2}. Cathode thickness is computed based on loading, specific capacity, and porosity. The choice of capacity loading establishes cell electrode area, which in turn fixes the material loading (g cm^{-2}) of the anode and cathode. Energy estimates assume that the cell develops the 16.7 Ah capacity with average cell voltage identical to the research cathode. Size and mass of the prismatic cell is determined using the material assumptions described previously. Power was estimated over a range of current density using a linear voltage relationship based on the data shown in Figure 2. Values of current density from 1 to 40 mA cm^{-2} were evaluated, creating the hypothetical Ragone diagrams in Figure 4. The choice of 40 mA cm^{-2} corresponds to the projected maximum power for the assumed linear voltage relationship (see Appendix A Figure A.3). Discharge performance data for Li-ion (based on the 18650 format LG MJ1 cell) is included for reference.

Projections require capacity loadings >2 mAh cm^{-2} to surpass the Li-ion benchmark of 230 Wh kg^{-1}. Combinations of high-specific capacity and loading approach 600 Wh kg^{-1} at low current density. Projected power density reaches 500 W kg^{-1} at about 5 mA cm^{-2}. Note that some combinations of the parameters selected for Figure 4 will be mutually exclusive in practice. The ability of the oxygen cathode to support high current density on the order of 5 to 10 mA cm^{-2}—while achieving the stated specific capacity at the cathode layer thicknesses shown—is uncertain and would require considerable advances in the state of the art for nonaqueous Li-O_2 cathodes. Nonetheless, the projections are useful for illustrating potential performance in the hypothetical cells with these physical assumptions.

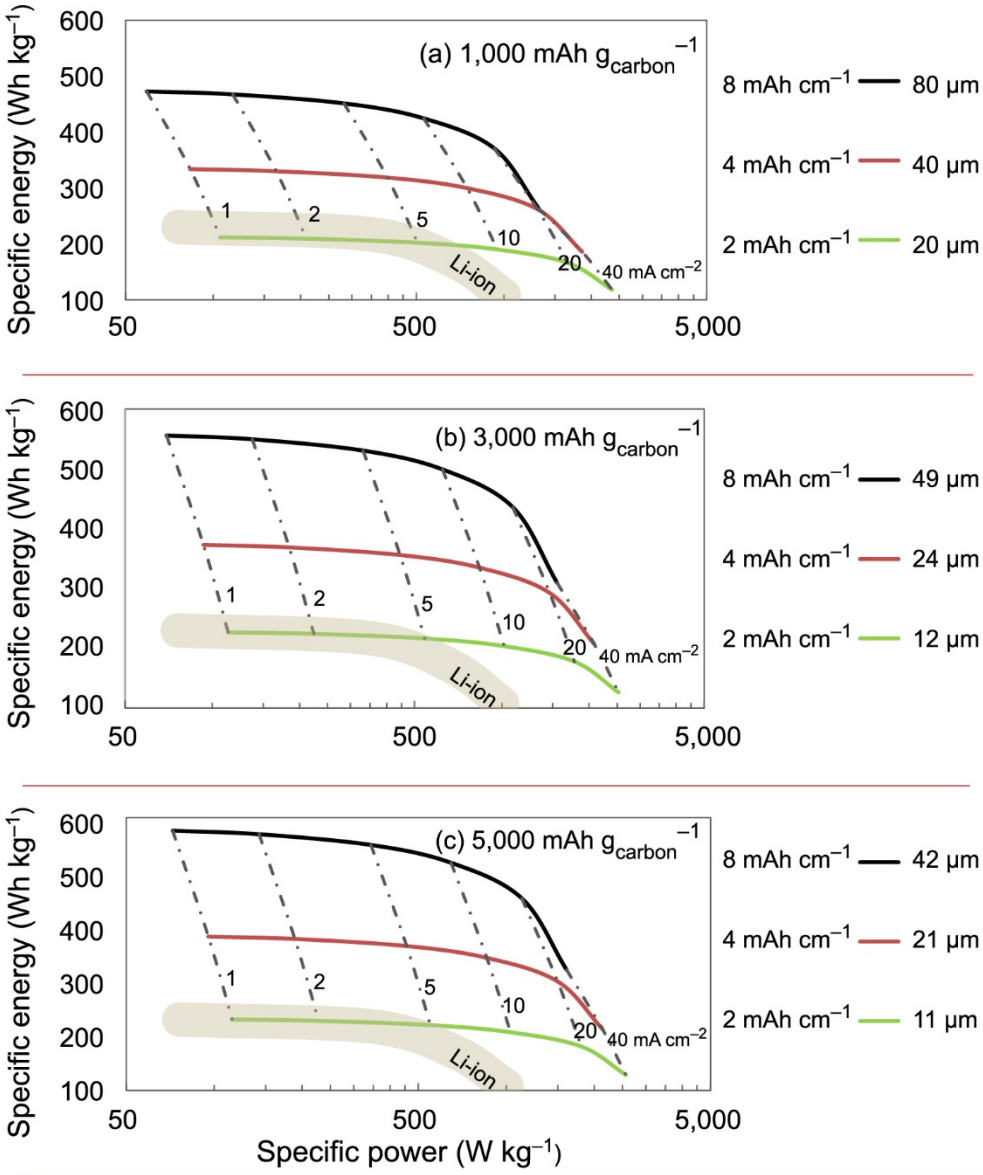

Figure 4.—Projected specific power and energy for 16.7 Ah prismatic cells at three levels of cathode specific capacity (a) 1,000, (b) 3,000, and (c) 5,000 mAh g_{carbon}^{-1} at three levels of capacity loading (2, 4, and 8 mAh cm^{-2}). Thickness in µm corresponds to associated cathode layer thickness. Projections are based on aggressive assumptions for current density and cell voltage (see text). Values include mass of stoichiometric oxygen. Dashed curves represent discharge current density 1 to 40 mA cm^{-2}.

A state of diminishing returns is apparent for values of cathode specific capacity greater than 3,000 mAh g^{-1}, because the cathode mass represents a relatively minor fraction of the cell components. Consider the projections at 4 mAh cm^{-2}. An increase in cathode capacity from 1,000 to 3,000 mAh g^{-1} increases specific energy from 330 to370 Wh kg^{-1}. Further gain in cathode specific capacity to 5,000 mAh g^{-1} produces a minor increase to 380 Wh kg^{-1}. An examination of the mass breakdown for these cells shows that the current collector material occupies significant mass. Because current collector (and separator) mass is proportional to electrode area, the electrode loading has a significant effect on the mass of nonactive cell materials and cell specific energy. Mass allocations for cells with 3,000 mAh g^{-1} cathodes are contrasted in Figure 5. Designed for 2 mAh cm^{-2}, the electrode area is 8,350 cm^2, and the current collector mass occupies 68 percent of the enclosed cell material, which limits specific energy to 230 Wh kg^{-1}. A heavier loading of 8 mAh cm^{-2} reduces the current collector mass to 31 percent increasing specific energy to 560 Wh kg^{-1}. Of course, the current collector design must be adequate to support the planned power requirements and current draw expected for the application. As expected, there is a tradeoff between specific power and energy. Optimization of the current collector with respect to current carrying capability is beyond the scope of this preliminary what-if analysis.

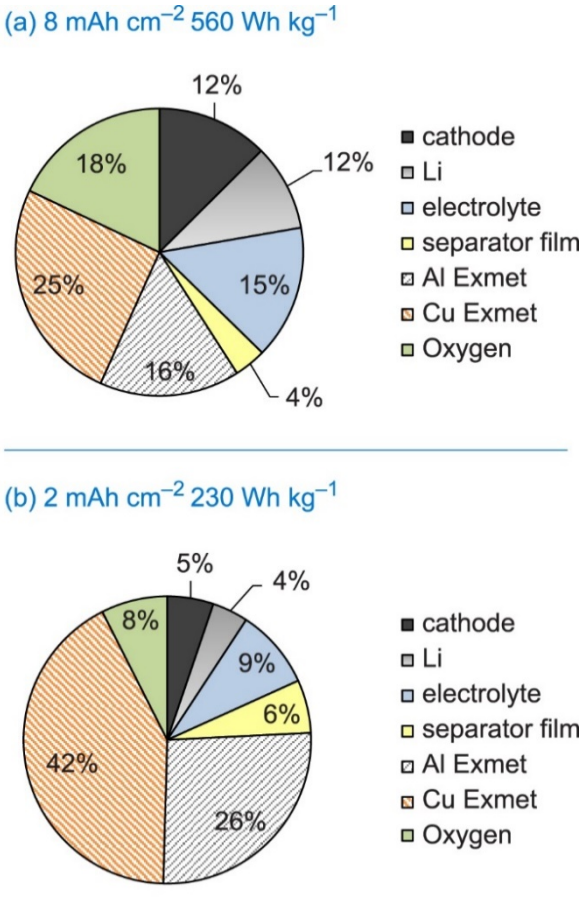

Figure 5.—Electrochemical material mass fraction for 3,000 mAh g^{-1} cathode material. Effect of capacity loading on relative mass of electrochemical materials. (a) Cell with loading of 8 mAh cm^{-2} achieves 560 Wh kg^{-1}. (b) Cell with loading of 2 mAh cm^{-2} achieves 230 Wh kg^{-1}. Cell enclosure, gas diffusion layer, and tab masses are not included in the specific energy calculations.

Similar sensitivity to loading and parasitic mass is presented by Park et al. for a lightweight folded cell design (see Ref. 37). The folded cells are projected to achieve >1,000 Wh kg^{-1} by omitting the anode current collector and using a lightweight, carbon paper gas diffusion layer (GDL) as an air flow field and cathode current collector. The addition of a copper current collector on the anode reduces their estimated specific energy to approximately 500 Wh kg^{-1}, belying the sensitivity of cell performance to the mass of inactive component materials. Moreover, their estimates do not appear to include oxygen mass or the weight of external cell structure.

Energy density is poor due to the relatively large internal volume occupied by the foam flow-field material. The 1.6-mm layer thickness selected for the gas flow field was approximately five times greater than the combined thickness of the electrodes, current collectors, and separator layers. This design choice limited the projected energy density to about 150 Wh L^{-1}, in contrast to >700 Wh L^{-1} for Li-ion. There is room for optimization in designing the flow field, but it is unlikely that Li-O_2 cells will compete favorably with Li-ion in terms of energy density.

We emphasize that the projections discussed previously are for single cells. Li-air and Li-O_2 batteries will introduce additional parasitic mass for structural components and power management and auxiliary systems similar to those used in a fuel cell balance of plant. Safety design features, which inhibit cell-to-cell thermal runaway would also add parasitic mass. Consequently, a practical metal-O_2 system will have to overcome challenging design issues in order to conserve the attractive specific energy and power suggested for individual cells.

5.0 Demonstration Cell and Pack Testing

5.1 Electric Flight Requirements

The LiON CAS project included work to evaluate the feasibility of developing a practical Li-O_2 battery for electric flight demonstrations with a small-scale experimental unmanned aerial vehicle (UAV). The goals for flight demonstration required a minimum flight time of 30 min with specific power >220 W kg^{-1}, including the mass of the aircraft. A battery-pack-level power requirement of 400 W at 24 V was identified for this application. Cells with 16.7 Ah capacity having 1C discharge rate capability were established as a design goal, with 10 cells in series to develop a minimum of 24 V under load. For reasons of safety and simplicity, the battery was designed to operate in air at ambient pressure and temperature. Testing was restricted to discharge only, because of known cycle life issues with carbon-based electrodes in organic electrolyte. Uncatalyzed carbon black cathode material was selected for demonstration purposes. All cell-level testing was performed in dry-room air with a dew point of approximately –40 °C, with 0.5 M LiTFSI and 0.5 M $LiNO_3$ in TEGDME as electrolyte.

5.2 Cathode Selection

Cathode performance was critical to this demonstration. As shown in the power relationship for the unoptimized laboratory cathode (see Figure 2(b)), the 400-W pack would require more than 3 m^2 of electrode material for a 24-V, 10-cell pack. This manufacturing scale was much greater than could be achieved in our laboratory; therefore, commercially available alternative cathode materials were explored for demonstration work. An emphasis was placed on discharge current density in order to minimize electrode area and mass of auxiliary cell materials, with a goal of at least 1 mA cm^{-2}.

Commercially available fuel cell GDLs with microporous layers (MPLs) offered one option for cathode scale up. The MPL typically consists of carbon black mixed with a PTFE binder and is materially very similar to the experimental laboratory cathodes (Ref. 45). Such materials are available in sheet sizes

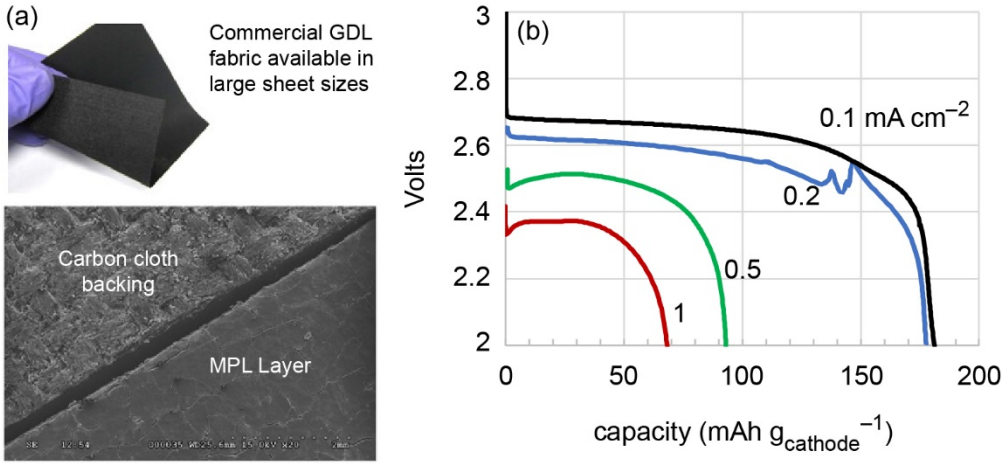

Figure 6.—(a) ELAT™ commercial gas diffusion layer (GDL). (b) Measured specific capacity based on total GDL mass including carbon cloth and MPL.

suitable for the large electrode area anticipated for demonstration. Testing showed that some of these GDLs could support discharge current densities on the order of ~1 mA cm^{-2}. ELAT™ LT1400W Carbon Cloth Electrode Material produced by NuVant Systems, obtained from Fuel Cells Etc was selected for scale-up work. This material provided a PTFE-bonded carbon black MPL with composition believed to be similar to the laboratory cathodes. The MPL was bonded to an electrically conductive carbon cloth layer (see Figure 6(a)). Thickness (400 μm) was similar to the FS laboratory cathodes. Areal density was 18 mg cm^{-2} including the mass of the carbon cloth, with specific capacity limited to 180 mAh g^{-1} at low current density (Figure 6(b)). This ersatz cathode material developed 70 mAh g^{-1} at the limiting current density of ~1 mA cm^{-2}, achieving 1.4 h of discharge time. Specific power and energy based on the dry mass of the ELAT™ material alone were limited to 110 and 460 Wh kg^{-1} respectively (see Appendix A Figure A.2). Because of the low performance metrics of available cathode materials, it was clear that a complete cell would not be able to achieve the 220 W kg^{-1} power goal for flight demonstration. Therefore, it was decided to limit demonstration work to subscale cells and stacks.

5.3 Demonstration Battery Pack Design

A passive, Li-air cell was assembled for laboratory demonstration purposes. Based on the prismatic design described previously, the prototype cells used three bicell elements with a total projected electrode area of 472 cm^2. Thin (127-μm) lithium foil anodes had a copper tab bonded to one side before sealing inside a 16-μm SETELA™ (Toray Industries, Inc.) separator. The thickness of lithium foil represented three times the capacity of the ELAT™ cathode, making the cells positive-limited. The excess thickness of lithium provided substantial electrical conductivity for a single discharge, making it unnecessary to provide a negative current collector. The embedded copper tab was required for making intercell electrical connections. ELAT™ cathodes used an aluminum Exmet current collector dispositioned over the carbon cloth side of the cathode. Reticulated polyester foam (3-mm thickness, 20 pores per inch) served as a gas distribution chamber between adjacent cathodes. Images of components and a cross section of the three-bicell structure with individual elements appears in Appendix A. The 60-g cells were not optimized for weight, achieving only 77 Wh kg^{-1} at low current density 0.1 mA cm^{-2}. Note that the limited cell-level specific energy was largely due to the relatively heavy case and low specific capacity of the ELAT™ cathode. Energy density for the prototype cells and pack proved to be poor (~40 Wh L^{-1}) due to the relatively large volume occupied by the reticulated foam flow field.

Cell layers were stacked by hand in dry-room air using a fixture to preserve alignment of the bicell elements and prevent short circuiting during assembly. Cathodes were wetted with 1 mL of electrolyte before stacking; therefore, the cells were active and at open circuit potential during and after assembly. The small cell size and low current-carrying capability of the cathode materials minimized the risks of live cell assembly.

A simple five-cell pack was assembled by joining five of the 470 cm^2 cells in series to construct a 12-V battery (see Figure 7). Testing was completed using a 50-min.-long profile, scaled down from projected powered flight requirements for the NASA X–57 Maxwell electric aircraft (Ref. 46). Power was scaled so that peak power intervals would be achieved at a current density of 0.8 mA cm^{-2}, representing approximately 80 percent of the limiting current observed in single-cell trials. This design choice was made to provide margin relative to the limiting current density of the cells in this design. Planned power segments for the prototype pack appear in Table 2. Testing was conducted at room temperature in quiescent "zero" air (<1 ppm CO_2, <1 ppm H_2O). The test objective was to demonstrate power-following capability with a simple Li-air design, at practical current density.

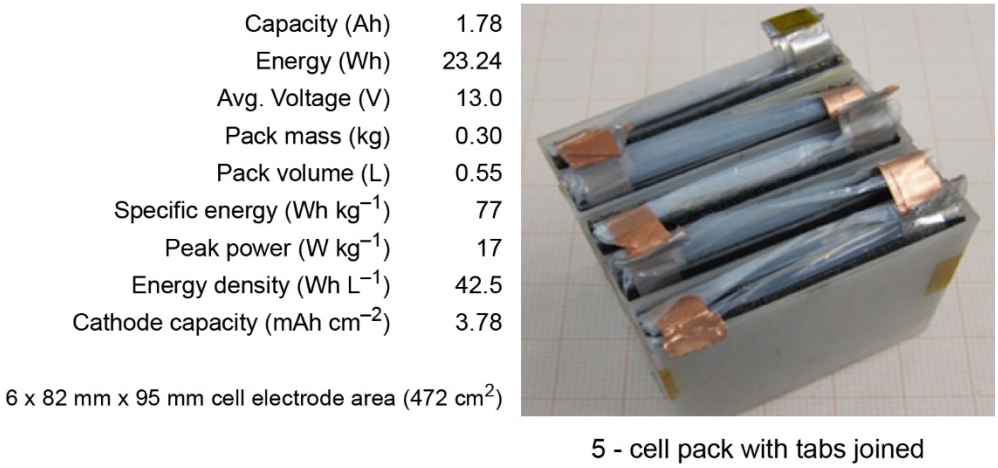

Figure 7.—Demonstration pack characteristics. Cells not optimized for mass. Discharge capacity and energy based on 0,1 mA cm^{-1} discharge in air using a 2 V cutoff.

TABLE 2.—FLIGHT DEMONSTRATION PACK POWER LEVELS SCALED TO 0.66 PERCENT OF X–57 LEVELS

Flight Segment	Duration, min.	X–57 power, kW	Scaled demonstration pack power, W	Current density, mA cm^{-2} approximately
Taxi from NASA	10	6.2	0.4	0.07
Takeoff checklist	2	0.8	0.1	0.01
Cruise runup	0.5	66.2	4.4	0.78
Flight go/no-go	0.5	0.8	0.1	0.01
Ground roll/climb	10.7	66.2	4.4	0.78
Cruise	5	49.8	3.3	0.59
Descent to 1,500 ft	7.5	17.1	1.1	0.20
Final approach	3	33.5	2.2	0.39
Rollout and turnoff	1	8.9	0.6	0.10
Taxi to NASA	10	6.2	0.4	0.07
Total time	50.2	---	---	-----

The passive Li-air pack demonstrated excellent load-following capability throughout the power profile achieving the transient response shown in Figure 8. The pack delivered 0.12 Ah and 1.43 Wh with average pack voltage of 11.9 V. Cell-to-cell voltage balance under power was within 100 mV throughout the discharge test. Cell voltage at 4.34 W maximum power (0.87 W per cell) was 2.25 V. Peak current reached approximately 0.38 A (0.8 A cm^{-2}) as planned. The calculated waste heat under this condition was ~0.39 W per cell, based on Equation (2). Heat generation is apparent in the temperature history of the pack, which revealed a 5 °C temperature rise in the interior cell during discharge (see Figure 8(b)). Cathode kinetics and ionic conductivity benefits would explain the observed increase in pack voltage at maximum power (see Figure 8(a)). Note that the 50-min. power profile required only 7 percent of the total 1.78 Ah capacity shown in Figure 7. The demonstration pack supported three consecutive discharge profiles without charging. Cell voltage balance deteriorated during the third power test.

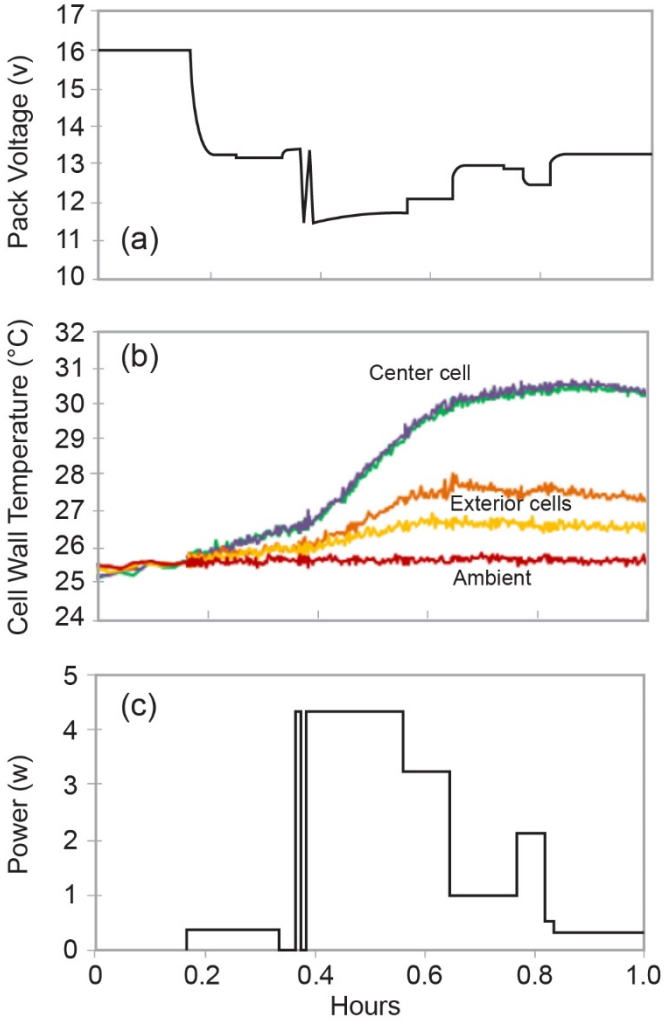

Figure 8.—Discharge performance of 12-V pack during power profile testing. The 50-min. test consumed 0.12 Ah capacity, delivering 1.43 Wh. Average current = 144 mA. (a) Pack voltage. (b) Cell surface temperature. (c) Discharge power history.

Without access to optimized materials the demonstration pack could not achieve the true potential for specific energy and power. Anode, cathode, flow field, and cell case were selected based on availability and cost. With optimization for mass, we believe the projections for 500 Wh kg^{-1} could be achieved at the cell level. The value of this demonstration pack was to display power-following capability in a scaled-up design with practical features.

6.0 Conclusions and Recommendations for Development

Projected power and energy characteristics for Li-O_2 cells with practical design elements are presented. These projections are based on optimistic estimates for cathode discharge performance and are presented as a what-if analysis. Assumptions included allowance for current collector materials, excess lithium capacity, and cell construction elements that would be common in a practical cell. Estimates suggest that specific energy could approach 400 to 600 Wh kg^{-1} at low current density for electrode loadings of 4 to 8 mAh cm^{-2}. Capacity loading of 4 mAh cm^{-2} is accomplished in practical Li-ion cells. However, nonaqueous Li-O_2 technology is partly at a disadvantage because the solid Li_2O_2 discharge product accumulates in the cathode pore structure where it interferes with rate capability and capacity. This makes it uncertain if the higher loadings assumed in making these estimates can be achieved.

Competitive levels of specific power will require capability for operation at high current density (5 mA cm^{-2} or greater). Cathode structure and electrolyte composition strongly influence this optimization (Refs. 47 to 49). A simple empirical model was used in this report to complete cell performance projections based on hypothetical cathode specific capacity and extrapolating voltage and current density from the experimental data of commercial (unoptimized) cathodes. Supplemental multiphysics simulations showed that by developing a cathode with a high-specific surface area and limiting the cathode thickness for maximum oxygen utilization can improve cathode rate capability. Multiphysics simulations allowed us to explore the optimization space, in one dimension, for better cathode designs that could match or improve the Li-O_2 cell projections further. Simulation results suggest a pathway towards high-specific energy and high-specific power cells enabled by using thin cathodes with a very high surface area and novel, ultralight current collectors (see Appendix B).

Practical metal-air batteries, like fuel cells, require a balance-of-plant to provide temperature control, safety monitoring, and fluid management. The cell-level projections in Figure 4 do not include the auxiliary mass of such supporting equipment. Possibly electric aircraft would have subsystems in place, which could be shared to provide air treatment and compression duties. However, the mass and parasitic power required for moisture and CO_2 removal components could be prohibitive and the loss of electrolyte solvent could remain problematic. A pressurized oxygen system could provide some relief from these complexities if explosion risks can be mitigated. The passive, prismatic cell that was explored in this report could lend itself to a pressurized oxygen design if adequate protection of the lithium metal can be achieved. Operation in oxygen could also be attractive in terms of rate capability and minimization of the gas flow-field volume. Safety issues associated with pressurized oxygen will require considerable attention before adoption in electric aviation applications.

Prospects for operation at elevated temperature need to be considered. It is possible that significant increases in rate capability (kinetics and transport) may be achieved if the cells are operated above room temperature (e.g., 100 °C). The efficiency of waste heat rejection would also be improved in elevated temperature systems. Inorganic electrolyte options such as ionic liquid materials or molten salts may achieve practical conductivity at elevated temperature and offer an option with reduced flammability.

Projections show that the path to improved specific energy and specific power require reduction in the mass of the inactive cell components. Ancillary components such as the separator and metallic current collector materials represent a significant fraction of the cell mass due to the relatively low mass occupied by high-specific capacity electrode materials (Figure 5). Approximately 50 percent of the cell material mass is occupied by metallic current collector materials. Mass savings can be accomplished by selecting lighter components or reducing the electrode area (operating at increased current density). The estimates presented in Figure 4 assumed commercially available, lightweight current collector materials. Efforts to reduce the collector mass need to be balanced against electrical resistance, making a significant reduction in current collector mass challenging for cells intended for high-power service.

Obstacles associated with cathode and electrolyte stability were considered separately in the LION project. The challenges for achieving satisfactory charge and discharge cycle life appear to be formidable. It remains to be seen if a viable cathode and electrolyte combination with adequate rate characteristics and cycle life can be developed.

Appendix A.—Material Evaluations

Appendix A presents some additional background information for the materials studied in the NASA Convergent Aeronautics Solutions (CAS) LION effort.

Candidate cathode materials were screened in 470 cm^2 cells (see Figure 3). Discharge voltage for the ELAT™ GDL material at constant current density is illustrated in Figure A.1. This material demonstrated poor discharge performance relative to the research cathode (see Figure 2). This shortfall in performance is partly due to the thickness and relatively heavy construction of the unoptimized GDL. Cell specific energy with this cathode material would necessarily be <180 Wh kg^{-1}.

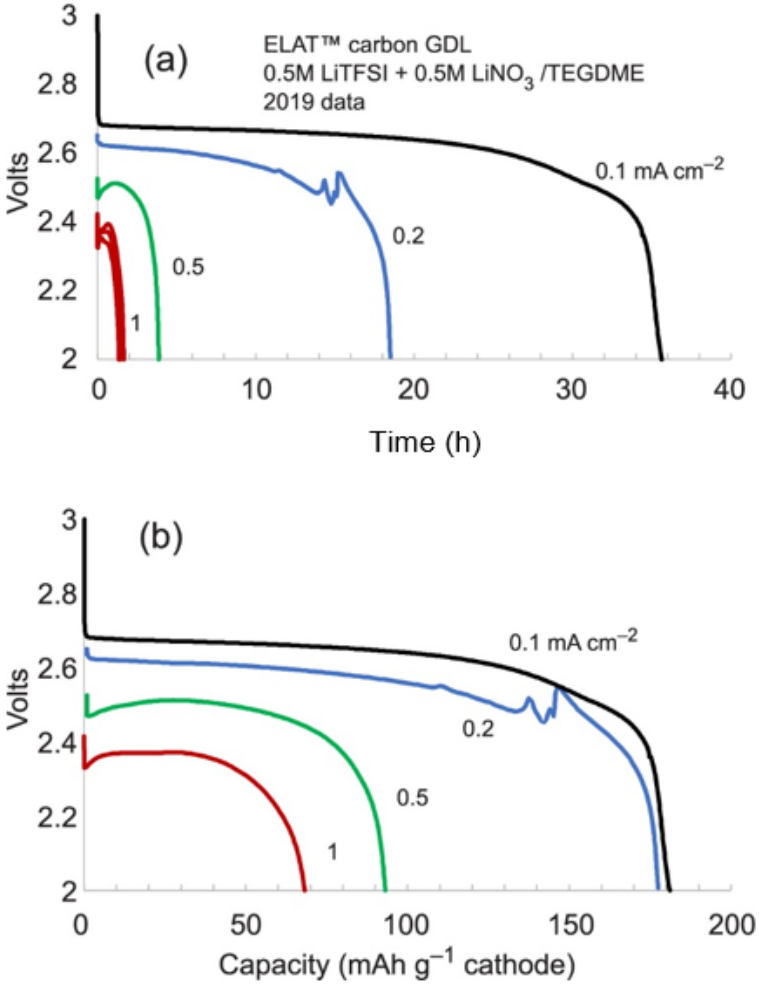

Figure A.1.—Discharge voltage profiles for commercial ELAT™ GDL as an air cathode. (a) Discharge time at constant current. (b) Specific capacity based on mass of cathode material. A momentary interruption in current produced the apparent discontinuity in the data at 0.2 mA cm^{-2}.

Discharge data in Figure A.2 is presented as equivalent specific power and specific energy in Figure A.2.

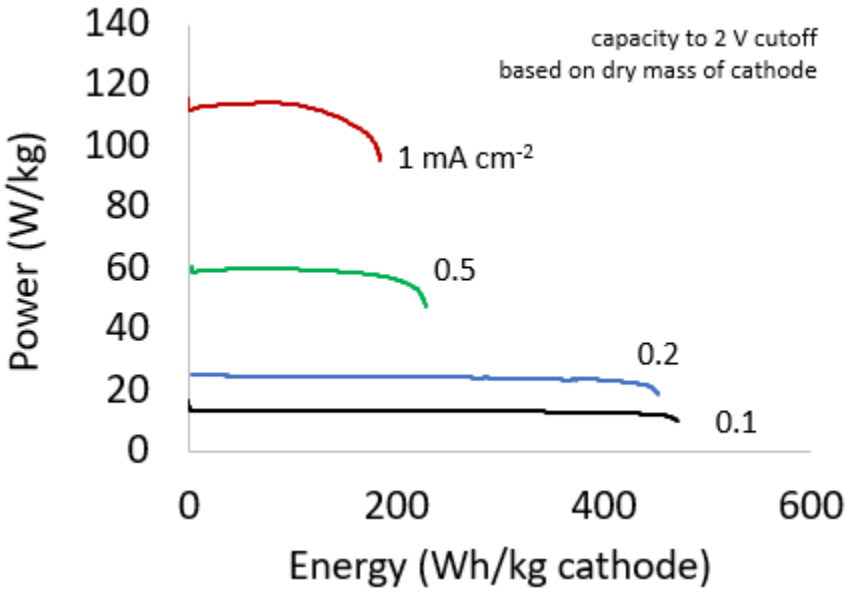

Figure A.2.—Computed specific power and energy based on the dry mass of ELAT™ GDL cathode material.

An extrapolation of the power characteristics for the $XC72_{FS}$ research cathode appears in Figure A.3. This projection assumes a constant ASI of 30 Ω-cm^2 with open-circuit voltage equal to 2.6 V. Hence, projected power follows a quadratic relationship with current. Projected peak power is 55 mW cm^{-2} at a current density of 40 mA cm^{-2}. In practice, kinetic and transport limitations would restrict the current density and voltage that is achieved.

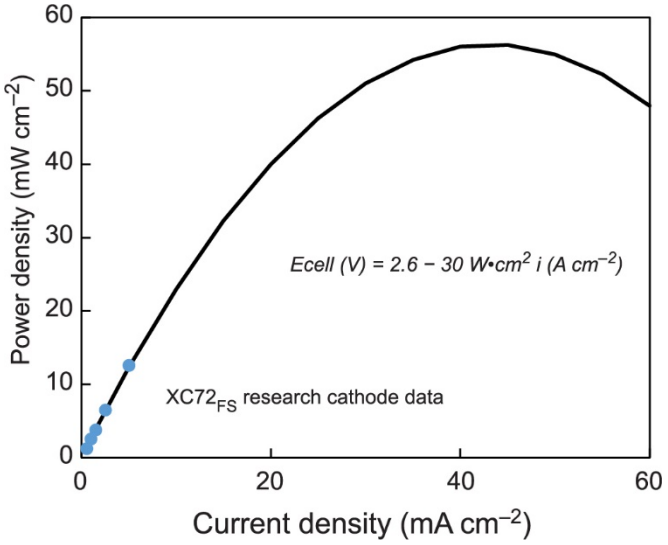

Figure A.3.—Extrapolated power density in W cm^{-2} based on linear voltage relationship with ASI = 30 Ω-cm^2 showing maximum at ~40 mA cm^{-2}. Blue symbols correspond to power data shown in Figure 2(b).

Cell components used in fabricating 470 cm^2 demonstration cells appear in Figure A.4. A cross section of the three-bicell assembly appears in Figure A.5.

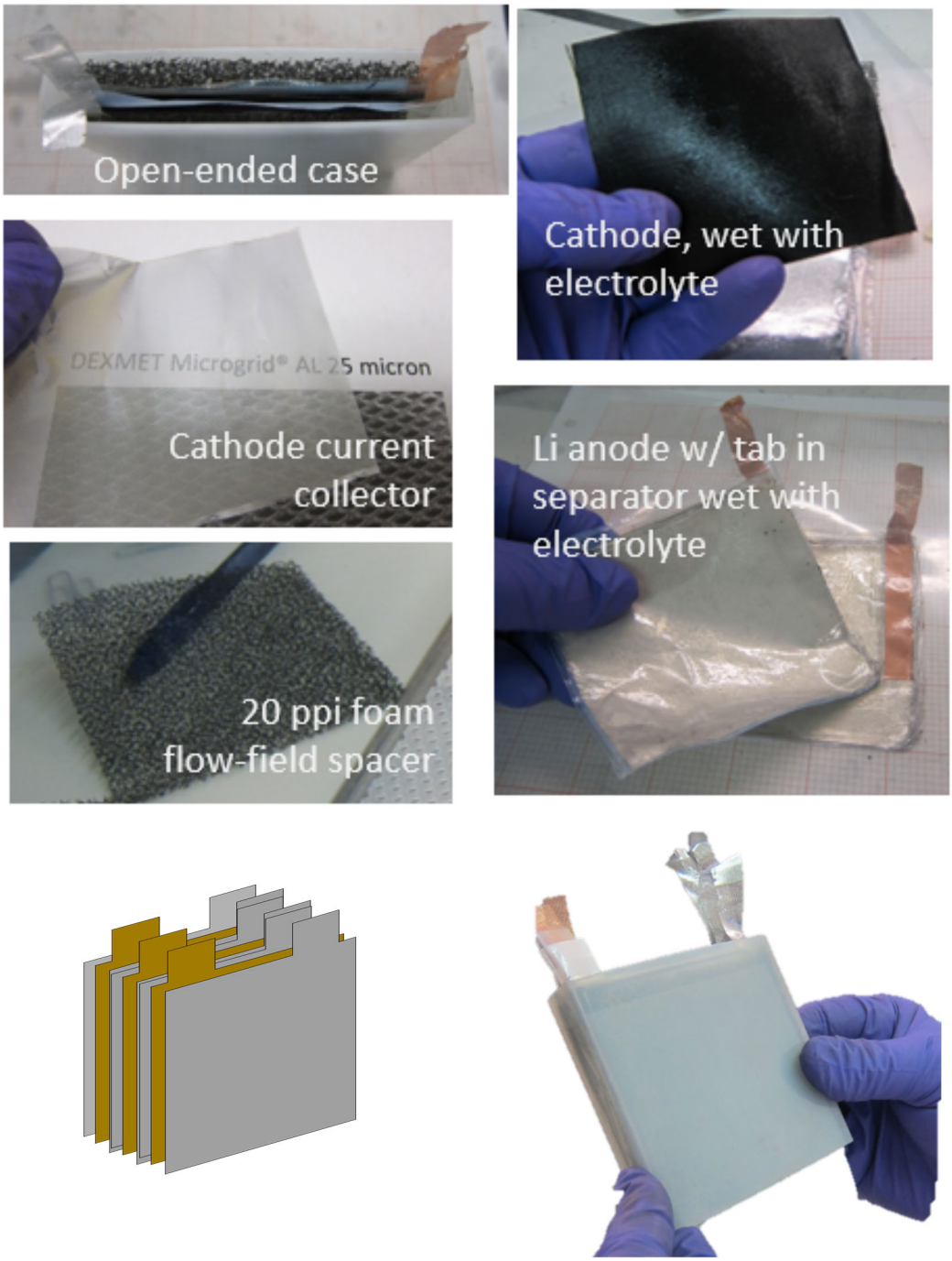

Figure A.4.—Bicell components for a 472 cm² demonstration cell. Bicell elements compressed and inserted into cell case. Tab edge and opposite edge of cell case are open to air. Finished cell mass approximately 60 g.

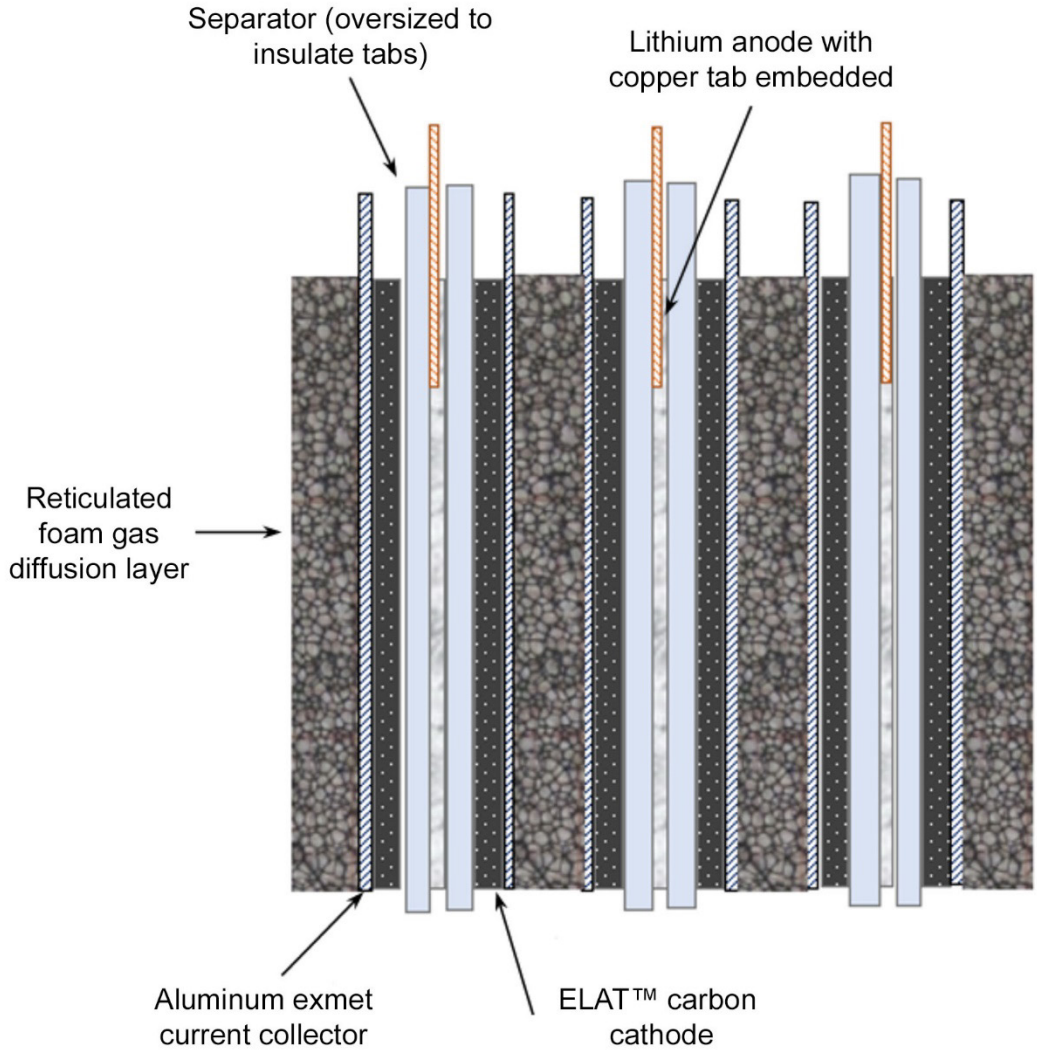

Figure A.5.—Cross-sectional schematic of demonstration cell with three bicell elements. Adjacent interior cathodes share one foam gas flow field. Both faces of the Li anode are utilized.

Mass estimates for Li-air cells with bicell construction included practical considerations for auxiliary materials and elements of construction. A list of assumptions appears in Table A.1. These assumptions produced a projected cell mass with approximately 20 percent structural material.

TABLE A.1.—PRISMATIC CELL MATERIALS AND PHYSICAL ASSUMPTIONS FOR SPECIFIC ENERGY ESTIMATION

Oxygen electrode	
carbon black	2.2 g cm^{-3}
binder	PVdF, 2 g cm^{-3}
porosity	6.9 cm^3 (110 percent of Li_2O_2 solid volume)
positive current collector	25-μm aluminum Exmet (40 percent open area)
	4 mg cm^{-2}, one 25-μm Exmet collector for each cathode sheet
Lithium metal electrode	
solid metal foil	thickness matched to cathode loading with 0.8 P N^{-1} capacity ratio
negative current collector	25-μm copper Exmet (40 percent open area), 14 mg cm^{-2}
	one 25-μm Exmet collector for each lithium bicell pair
Separator	16-μm polyolefin film
Electrolyte	1M LiTFSI in TEGDME
Cell construction	
30 bicell elements	1.5:1 aspect ratio
Case material	0.1-mm aluminum laminate
	laminated pouch cell film, 36 mg cm^{-2}
Gas flow-field material	Reticulated polyurethane foam, 20 ppi, 8 mg cm^{-2}
	3.2-mm (1/8-in.) thickness, compressed to 1.6 mm
Auxiliary materials	
Tabs	1.27 cm by 1/8 of electrode width (approx. 1 g total)
Terminals	27-μm nickel foil, 1.2 cm width by 1.27 cm length, 0.73 g total
	calculated resistance: 3 mΩ each
Cover material	0.5 g

Appendix B.—Multiphysics Projections for Cathode Performance

Metal-air battery chemistry in the organic electrolyte is often limited by diffusion of oxygen in the electrolyte. The diffusivity of oxygen in organic and polymer electrolytes is low compared to oxygen in the aqueous electrolytes (aqueous Li-air) or electrode structure (such as a three-phase boundary in a fuel cell). We can use an understanding of this limited diffusivity (Ref. 47) to our advantage to design an optimal cathode to reduce cell mass without compromising on cell power. The model and simulation methodology are discussed in detail in Reference 49. In addition to the mass of electrolyte, carbon particles, binder, separator, and lithium anode, we included the mass of lithium peroxide in the cathode, the mass of the oxygen in the cathode and separator, and mass of the state-of-the-art current collectors. The total cell mass is calculated in the following way. The mass of the dissolved oxygen in the electrolyte

$$m_{O2} = M_{O2} c_{O2} \left(\epsilon_{elyte}^{cat} V_{cat} + \epsilon_{elyte0}^{sep} V_{sep} \right)$$

where m_{O2} is the mass of oxygen, M_{O2} is the molar mass of oxygen, c_{O2} is the concentration of dissolved oxygen in the electrolyte, ϵ_{elyte}^{cat} is the volume fraction of the electrolyte in the cathode at the end of discharge, V_{cat} is the volume of the cathode, ϵ_{elyte0}^{sep} is the initial volume fraction of the electrolyte in the separator, and V_{sep} is the volume of the separator. The mass of the deposited lithium peroxide

$$m_{Li2O2} = \epsilon_{Li2O2} V_{cat} \times 2.31 \text{ g cm}^{-3}$$

where ϵ_{Li2O2} is the average volume fraction of the deposited product inside the porous cathode at the end of discharge. The mass density of lithium peroxide is taken as 2.31 g cm^{-3}. The mass of the electrolyte is computed as

$$m_{elyte} = \dot{m_{elyte}} \left(\epsilon_{elyte}^{cat} V_{cat} + \epsilon_{elyte0}^{sep} V_{sep} \right)$$

where $\dot{m_{elyte}}$ is the mass density of the electrolyte. The mass density for a 1M LiTFSI in DME was taken as 1.041 g cm^{-3}. The mass of the carbon was computed using

$$m_{carbon} = \dot{m_{carbon}} \epsilon_{carbon} V_{cat}$$

where $\dot{m_{carbon}}$ is the mass density of carbon particles (2.26 g cm^{-3}), $\epsilon_{carbon} = \left(1 - \epsilon_{elyte0}^{cat}\right)$ is the volume fraction of carbon (assuming negligible binder). The mass of the separator is

$$m_{sep} = \epsilon_{sep} V_{sep} \dot{m_{sep}}$$

where $\dot{m_{sep}} \doteq 2.648$ g cm^{-3} is the mass density of the separator. The anode mass, assuming optimistic anode architecture such as a copper current collector with a porous structure for housing lithium (Ref. 50)

$$m_{\text{3D-anode}} = \left(\frac{\dot{m_{Li2O2}} M_{eLi}}{\dot{m_{Li}} M_{Li2O2}} \right) \times \dot{m_{\text{3D-anode}}} \times \epsilon_{Li2O2} V_{cat}$$

where the mass density of three-dimensional (3D) anode ($\dot{m_{\text{3D-anode}}}$) is 0.8 g cm^{-3}, where the last part of the equation is the amount of lithium required to form lithium peroxide. Finally, the mass of an optimistic cathode current collector

$$m_{cc} = 1.91 \text{ g cm}^{-3} \times 4 \text{ μm} \times A_{cross}$$

where the optimal thickness of the cathode current collector was assumed to be 4 μm (Ref. 51) and the mass density of the rGO (reduced Graphene Oxide) to be 1.91 g cm^{-3}. The total mass of the optimistic Li-O_2 without the oxygen supply infrastructure

$$m_{\text{total}} = m_{\text{3D-anode}} + m_{sep} + m_{elyte} + m_{carbon} + m_{Li2O2} + \text{m}_{\text{O2}} + m_{\text{CC}}$$

The optimal simulations were performed using the grid approach, discussed in detail in Reference 50. A range of values for cathode thickness (10 to 400 μm), cathode porosity (0.4 to 0.8), and discharge current density (0.5 to 5 mA cm^{-2}) were simulated. The mass and power were computed at each simulation tuple, resulting in a value of specific power and specific energy. The maximum values of specific power and specific energy was used to plot Figure B.1.

The results are shown for 1M LiTFSI in DME at p_{O_2} = 1,100 torr. The simulation conditions match the experimental conditions (Figure 2) and the empirical model (Fig. B.1) discussed in the main report. The high-specific energy cells result in thicker cathodes about 180 μm at a lower value of the discharge current density, 0.5 mA cm^{-2}. In contrast, high-specific power cells have very thin cathodes, about 10 μm, with high values of the discharge current density, 5 mA cm^{-2}, and short discharge times ranging from 1 to 10 min. The high-specific energy cells can discharge for more than 50 h, while the high-specific power cells would fully discharge in less than 5 min. Note that this multiphysics calculation represents an upper limit for specific energy based on a minimum of ancillary cell material. This calculation does not include the parasitic mass of a cell case, tab connections, gas flow field, or excess anode material.

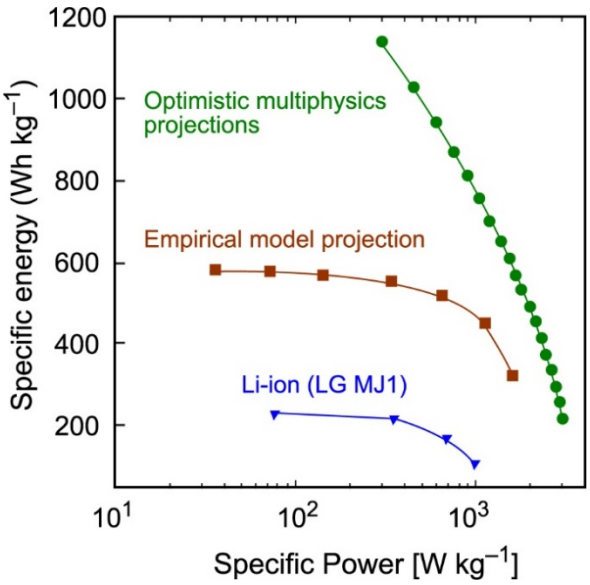

Figure B.1.—Ragone plot comparing Li-O_2 performance for 1M LiTFSI in DME at p_{O_2} = 1,100 torr using fully coupled differential equations from References 50 and 51 (green), the empirical model (brown, best projection from). Data for the lithium-ion chemistry is taken from in-house testing of LG MJ1 high-energy 18650 format cells.

References

1. Schäfer, A.W., et al.: Technological, Economic and Environmental Prospects of All-Electric Aircraft. Nat. Energy, vol. 4, 2019, pp. 160–166.
2. Anderson, Natalie; Tran, Minh; and Darcy, Eric: 18650 Cell Bottom Vent: Preliminary Evaluation Into Its Merits for Preventing Side Wall Rupture. Presented at the NASA-JSC S&T Meeting, San Diego, CA, 2016.
3. Christensen, J., et al.: A Critical Review of Li/Air Batteries. J. Electrochem. Soc., vol. 159, no. 2, 2012, pp. R1–R30.
4. Qian, Jiangfeng, et al.: High Rate and Stable Cycling of Lithium Metal Anode. Nat. Commun., vol. 6, no. 6362, 2015.
5. Luntz, Alan C.; and McCloskey, B.D.: Nonaqueous Li–Air Batteries: A Status Report. Chem. Rev. vol. 114, no. 23, 2014, pp. 11721−11750.
6. Gallagher, Kevin G., et al.: Quantifying the Promise of Lithium–Air Batteries for Electric Vehicles. Energy Environ. Sci., vol. 7, no. 5, 2014, p. 1555.
7. Fredericks, William L., et al.: Performance Metrics Required of Next-Generation Batteries to Electrify Vertical Takeoff and Landing (VTOL) Aircraft. ACS Energy Lett., vol. 3, 2018, pp. 2989−2994.
8. Kuhn, H.; and Sizmann, A.: Fundamental Prerequisites for Electric Flying. Deutscher Luft- und Raumfahrtkongress 2012, 2012.
9. Dornbusch, Donald A., et al.: Development of Cathode and Electrolyte Materials for Lithium-Oxygen Batteries for Electric Aviation. The Electrochemical Society MA2019-02 585, 2019.
10. Dornbusch, Donald A; Viggiano, Rocco P.; and Lvovich, Vadim F.: Integrated Impedance-NMR Identification of Electrolyte Stability in Lithium-Air Batteries. Electrochim. Acta, vol. 349, no. 136169, 2020.
11. McCloskey, Bryan D., et al.: Mechanistic Insights for the Development of Li–O_2 Battery Materials: Addressing Li_2O_2 Conductivity Limitations and Electrolyte and Cathode Instabilities. Chem. Commun., vol. 51, 2015, pp. 12701–12715.
12. Viswanathan, V., et al.: Li−O_2 Kinetic Overpotentials: Tafel Plots From Experiment and First-Principles Theory. J. Phys. Chem. Lett., vol. 4, no. 4, 2013, pp. 556−560.
13. Margulies, Benjamin; and Read, Jeffrey: Carbon/PTFE Electrode for Lithium/Air-Water Batteries. ARL–TR–4066, 2007.
14. Ji, M.B., et al.: A More Flooding-Tolerant Oxygen Electrode in Alkaline Electrolyte. Fuel Cells, vol. 10, no. 2, 2010, p. 289.
15. Kraytsberg, Y. Ein-Eli: Review on Li–Air Batteries—Opportunities, Limitations and Perspective. J. Power Sources, vol. 196, 2011, pp. 886–893.
16. Li, X.; Huang, J.; and Faghri, A.: A Critical Review of Macroscopic Modeling Studies on Li O_2 and Li-Air Batteries Using Organic Electrolyte: Challenges and Opportunities. J. Power Sources, vol. 332, 2016, pp. 420–446.
17. Xia, Chun, et al.: Evolution of Li_2O_2 Growth and Its Effect on Kinetics of Li–O_2 Batteries. ACS Appl. Mater. Interfaces, vol. 6, no. 15, 2014, pp. 12083–12092.
18. Burke, Colin M., et al.: Enhancing Electrochemical Intermediate Solvation Through Electrolyte Anion Selection to Increase Nonaqueous Li–O_2 Battery Capacity. PNAS, vol. 112, no. 30, 2015, pp. 9293–9298.
19. Adams, Brian D., et al.: Current Density Dependence of Peroxide Formation in the Li–O_2 Battery and Its Effect on Charge. Energy Environ. Sci., no. 6, 2013, pp. 1772–1778.

20. Lim, Hyung-Kyu, et al.: Toward a Lithium−"Air" Battery: The Effect of CO_2 on the Chemistry of a Lithium−Oxygen Cell. J. Am. Chem. Soc., vol. 135, no. 26, 2013, pp. 9733−9742.
21. McCloskey, Bryan D., et al.: Combining Accurate O_2 and Li_2O_2 Assays to Separate Discharge and Charge Stability Limitations in Nonaqueous Li–O_2 Batteries. J. Phys. Chem. Lett., vol. 4, no. 17, 2013, pp. 2989–2993.
22. McCloskey, Bryan D., et al.: Twin Problems of Interfacial Carbonate Formation in Nonaqueous Li–O_2 Batteries. J. Phys. Chem. Lett., vol. 3, no. 8, 2012, pp. 997–1001.
23. McCloskey, Bryan D., et al.: Mechanistic Insights for the Development of Li–O_2 Battery Materials: Addressing Li_2O_2 Conductivity Limitations and Electrolyte and Cathode Instabilities. Chem. Commun., vol. 51, 2015, pp. 12701–12715.
24. Thotiyl, Muhammed M. Ottakam, et al.: The Carbon Electrode in Nonaqueous Li-O_2 cells. J. Am. Chem. Soc., vol. 135, no. 1, 2013, pp. 494–500.
25. Mahne, Nika, et al.: Mechanism and Performance of Lithium-Oxygen Batteries—A Perspective. Chem. Sci., vol. 8, 2017, pp. 6716–6729.
26. Itkis, Daniil M., et al.: Reactivity of Carbon in Lithium–Oxygen Battery Positive Electrodes. Nano Lett., vol. 13, no. 10, 2013, pp. 4697–4701.
27. Aurbach, Doron, et al.: Advances in Understanding Mechanisms Underpinning Lithium–Air Batteries. Nat. Energy, vol. 1, no. 16128, 2016.
28. Sharon, Daniel, et al.: 2,4-Dimethoxy-2,4-dimethylpentan-3-one: An Aprotic Solvent Designed for Stability in Li–O_2 Cells. J. Am. Chem. Soc., vol. 139, no. 34, 2017, 11690–11693.
29. Kwak, Won-Jin, et al.: Li–O_2 Cells With LiBr as an Electrolyte and a Redox Mediator. Energy Environ. Sci., vol. 9, 2016, pp. 2334–2345.
30. Lim, H.-D., et al.: Reaction Chemistry in Rechargeable Li–O_2 Batteries. Chem. Soc. Rev., vol. 46, 2017, pp. 2873–2888.
31. Adams, James; Karulkar, Mohan; and Anandan, Venkataramani: Evaluation and Electrochemical Analyses of Cathodes for Lithium-Air Batteries. J. Power Sources, vol. 239, 2013, pp. 132–143.
32. Walker, Wesley, et al.: A Rechargeable Li–O_2 Battery Using a Lithium Nitrate/N,N-Dimethylacetamide Electrolyte. J. Am. Chem. Soc., vol. 135, no. 6, 2013, pp. 2076–2079.
33. Bryantsev, Vyacheslav S., et al.: Investigation of Fluorinated Amides for Solid-Electrolyte Interphase Stabilization in Li-O_2 Batteries Using Amide-Based Electrolytes. J. Phys. Chem. C, vol. 117, no. 23, 2013, pp. 11977–11988.
34. Greszler, Thomas A.: Li-Air and Li-Sulfur Technology in an Automotive System Context. Beyond Lithium Ion 5, Berkeley Lab, Berkeley, CA, 2012.
35. Linden, David; and Reddy, Thomas B.: Handbook of Batteries. Third Ed., Ch. 32, McGraw-Hill, New York, NY, 2002.
36. Safety Standard for Oxygen and Oxygen Systems: Guidelines for Oxygen System Design, Materials Selection, Operations, Storage, and Transportation. NSS–1740.15, 1996.
37. Park, Jung O., et al.: A 1000 Wh kg-1 Li-Air Battery: Cell Design and Performance. J. Power Sources, vol. 419, 2019, pp. 112–118.
38. Liyana-Arachchi, Thilanga P., et al.: Polarizable Molecular Dynamics and Experiments of 1,2-Dimethoxyethane Electrolytes With Lithium and Sodium Salts: Structure and Transport Properties. J. Phys. Chem. B, vol. 122, no. 36, 2018, pp. 8548–8559.
39. Radhakrishnan, R.G., et al.: First Principles Computational and Experimental Investigation of Molten Salt Electrolytes: Implications for Li-O_2 Batteries. J. Phys. Chem. C, 2020, pending final review.
40. Knudsen, K.B., et al.: Calphad Modeling and Experimental Evaluation of New Molten Salt Mixtures for Li-O_2 Batteries. J. Phys. Chem. C, 2019, in preparation.

41. McCloskey, Bryan D., et al.: On the Efficacy of Electrocatalysis in Nonaqueous Li–O_2 Batteries. J. Am. Chem. Soc., vol. 133, no. 45, 2011, pp. 18038–18041.
42. Knudsen, Kristian B., et al.: An Electrochemical Impedance Spectroscopy Study on the Effects of the Surface- and Solution-Based Mechanisms in Li-O_2 Cells. J. Electrochem. Soc., vol. 163, no. 9, 2016, pp. A2065–A2071.
43. Moshtev, R.; and Johnson, B.: State of the Art of Commercial Li Ion Batteries. J. Power Sources, vol. 91, no. 2, 2015, pp. 86–91.
44. Jung, Hun-Gi, et al.: An Improved High-Performance Lithium-Air Battery. Nat. Chem., vol. 4, 2012, pp. 579–585.
45. Tanuma, T.: Innovative Hydrophilic Microporous Layers for Cathode Gas Diffusion Media. J. Electrochem. Soc., vol. 157, no. 12, 2010, pp. B1809–B1813.
46. Schnulo, Sydney L., et al.: Development of a Multi-Phase Mission Planning Tool for NASA X–57 Maxwell. Presented at the AIAA Aviation Forum, Atlanta, GA, 2018.
47. Mehta, M.; Bevara, V.; and Andrei, P.: Maximum Theoretical Power Density of Lithium–Air Batteries With Mixed Electrolyte. J. Power Sources, vol. 286, 2015, pp. 299–308.
48. Liu, Jing; Rahimian, Saeed Khaleghi; and Monroe, Charles W.: Capacity-Limiting Mechanisms in Li/O_2 Batteries. Phys. Chem. Chem. Phys., vol. 18, 2016, pp. 22840–22851.
49. Mehta, Mohit R., et al.: Li-O_2 Batteries for High Specific Power Applications: A Multiphysics Simulation Study for a Single Discharge. J. Power Sources, vol. 484, no. 229261, 2021.
50. Yun, Qinbai, et al.: Chemical Dealloying Derived 3D Porous Current Collector for Li Metal Anodes. Adv. Mater., vol. 28, no. 32, 2016, pp. 6932–6939.
51. Chen, Y., et al.: Reduced Graphene Oxide Films With Ultrahigh Conductivity as Li-Ion Battery Current Collectors. Nano Lett., vol. 16, no. 6, 2016, pp. 3616–3623.